The Hydrogen Bonds between Arg^{423} and Glu^{472} and Other Key Residues, Asp^{443}, Ser^{477}, and Pro^{489}, Are Responsible for the Formation and a Different Positioning of TNP-ATP and ATP within the Nucleotide-Binding Site of Na^+/K^+-ATPase†

Zdeněk Lánský,‡,§ Martin Kubala,‡,§ Rüdiger Ettrich,|| Michal Kutý,|| Jaromír Plášek,§ Jan Teisinger,‡ Wilhelm Schoner,⊥ and Evžen Amler*,‡,▽

Institute of Physiology, Czech Academy of Sciences, Vídeňská 1083, 14220 Prague, Czech Republic, Institute of Physics, Charles University of Prague, Ke Karlovu 5, 12116 Prague, Czech Republic, Laboratory of High Performance Computing, Institute of Physical Biology USB and Institute of Landscape Ecology of AS CR, Zámek 136, 37333 Nové Hrady, Czech Republic, and Institute of Biophysics, 2nd Faculty of Medicine, Charles University, V Úvalu 84, 15006 Praha 5, Czech Republic, and Institute of Biochemistry and Endocrinology, Justus-Liebig-University Giessen, Frankfurter Strasse 100, D-35392 Giessen, Germany

Received February 17, 2004; Revised Manuscript Received April 15, 2004

ABSTRACT: Mutation of Arg^{423} at the N-domain of Na^+/K^+-ATPase resulted in a large decrease of both TNP-ATP and ATP binding. Thus, this residue, localized outside the binding pocket, seems to play a key role in supporting the proper structure and shape of the binding site. In addition, mutation of Glu^{472} also caused a large decrease of both TNP-ATP and ATP binding. On the basis of our computer model, we hypothesized that a hydrogen bond between Arg^{423} and Glu^{472} supports the connection of two opposite halves of the ATP-binding pocket. To verify this hypothesis, we have also prepared the construct containing both these mutations. Binding of neither TNP-ATP nor ATP to this double mutant differed from binding to any of the single mutants. This strongly supported the existence of the hydrogen bond between Arg^{423} and Glu^{472}. Similarly, the conserved residue Pro^{489} seems to be substantial for the proper interaction of the third and fourth β-strands of the N-domain, which both contain residues that take part in ATP binding. Mutation of Asp^{443} affected only ATP, but not TNP-ATP, binding, suggesting that these ligands adopt different positions in the nucleotide-binding pocket. On the basis of a recently published crystal structure [Håkansson, K. O. (2003) *J. Mol. Biol. 332*, 1175−1182], we improved our model and computed the interaction of these two ligands with the N-domain. This model is in good agreement with all previously reported spectroscopic data and revealed that Asp^{443} forms a hydrogen bond with the NH_2 group of the adenosine moiety of ATP, but not TNP-ATP.

Na^+/K^+-ATPase[1] is an enzyme of the plasma membrane exporting three sodium ions out of the cell and importing two potassium ions into it per ATP split (*1*, *2*). Its energy of hydrolysis leads to conformational changes of the catalytic α-subunit (∼110000 Da) and to the vectorial process. The β-subunit, a glycoprotein of ∼55000 Da, seems to be involved in the proper folding and trafficking of the enzyme and may contain parts of the cation ionophore (*1*−*3*). Despite a huge body of information, it is not understood so far on a molecular level how ATP hydrolysis is converted to vectorial transport.

Significant progress in understanding this process comes from the recent elucidation of the crystal structure of another P-type ATPase (*1*) in two different conformational states, the Ca^{2+}-ATPase of the sarcoplasmic reticulum (SERCA) (*4*, *5*). Three well-separated domains exposed to the cytoplasm could be identified which move toward each other. They were designated according to their proposed function as A (actuator or anchor), N (nucleotide binding), and P (phosphorylation). SERCA shows 30% identity and 65% similarity to Na^+/K^+-ATPase. In analogy to Ca^{2+}-ATPase, cryoelectron microscopy on crystals of Na^+/K^+-ATPase with 9 Å resolution (*6*) showed three large domains exposed to the cytoplasm. Sweadner and Donnet (*7*) analyzed the structure of SERCA in the E1 conformation in terms of corresponding residues in Na^+/K^+-ATPase. They estimated that all residues known as cleavage sites for trypsin, chymotrypsin, or Pronase are located on the surface of the enzyme, except for those on the H_9-H_{10} loop. Fragments

† This work has been supported by the Ministry of Education, Youth and Sports of the Czech Republic (Project Nos. LN 00A141 and 113100001), by the Grant Agency of the Czech Republic (Project Nos. 206/03/D082, 309/02/1479, and 305/03/H148), and by Research Project AVOZ 5011922.

* To whom correspondence should be addressed. E-mail: amler@biomed.cas.cz.

‡ Institute of Physiology, Czech Academy of Sciences.

§ Institute of Physics, Charles University of Prague.

|| Institute of Physical Biology USB and Institute of Landscape Ecology of AS CR.

⊥ Justus-Liebig-University Giessen.

▽ 2nd Faculty of Medecine, Charles University of Prague.

[1] Abbreviations: ATP, adenosine 5′-triphosphate; D443A, aspartic acid on position 443 was replaced by alanine, other mutations analogously; GST, glutathione-S-transferase from *Schistosoma japonicum*; H_1-H_{10}, transmembrane helices numbered from the NH_2-terminal end of the peptidic chain; K_A, dissociation constant for ATP; K_P, dissociation constant for the fluorescent probe; Na^+/K^+-ATPase, Na^+ and K^+ transporting adenosine 5′-triphosphatase (EC 3.6.1.37); SERCA, Ca^{2+}-ATPase from the sarco(endo)plasmic reticulum (EC 3.6.1.38); TNP-ATP, 2′,3′-*O*-(2,4,6-trinitrophenyl)adenosine 5′-triphosphate, trisodium salt.

10.1021/bi0496485 CCC: $27.50
Published on Web 06/10/2004

obtained by Fe^{2+}-oxidative cleavage of Na^+/K^+-ATPase (*8*) were also consistent with the structure found for SERCA. Furthermore, they confirmed that the position of all cysteine residues, which were successfully labeled in experiments with Na^+/K^+-ATPase, correspond to the residues on the surface of the enzyme. These findings support the idea that the topologies of the catalytic subunit of SERCA and Na^+/K^+-ATPase are very similar.

The single ATP-binding site was identified on the N-domain. It is constituted by the central part of the major cytoplasmic loop connecting transmembrane helices 4 and 5 (roughly Arg^{378}−Arg^{589}) (*9*). Using the protein-reactive ATP analogues 2-azido-ATP (*10*) and 8-azido-ATP (*11*), it was possible to label and identify Gly^{502} and Lys^{480}, respectively, as possible recognition sites for ATP. The facts that ATP prevents modification of Lys^{501} by fluorescein 5′-isothiocyanate (FITC) (*12*) and that fluorescence of FITC attached to this residue cannot be quenched by antifluorescein (*13*) led to the conclusion that Lys^{501} is localized in the depth of the ATP-binding pocket. Development of molecular biology brought a new efficient way for examining the role of individual amino acids in the ATP interaction with the enzyme. Mutagenesis studies confirmed the important roles of Lys^{480} (*14*) and Lys^{501} (*15*). Furthermore, it was shown that mutation of Glu^{446} (*16*), Phe^{475} (*15*, *16*), and Gln^{482} (*17*) also substantially inhibited ATP binding. A recently published structure of the N-domain estimated by NMR detected a hydrogen bond between Gln^{482} and the adenosine moiety of ATP; moreover, the backbone oxygen of Ala^{503} also contributed to ATP binding (*18*).

An NMR study of the isolated Thr^{357}−Leu^{600} segment of SERCA (corresponding to the N-domain) showed that Glu^{439}, Ser^{488}, and Val^{514} are influenced by nucleotide binding (*19*); the corresponding residues in Na^+/K^+-ATPase are Asp^{443}, Ser^{477}, and Met^{500}, respectively. Moreover, Fe^{2+}-oxidative cleavage of Na^+/K^+-ATPase suggested that Asp^{443} plays an important role in ATP binding and/or phosphorylation of the enzyme (*8*). The homology modeling of the H_4−H_5 loop predicted that Ser^{477} could participate in ATP binding (*9*). Finally, the Met^{500} is closely connected to the important region Lys^{501}−Ala^{503}. Using site-directed mutagenesis, we mutated Asp^{443}, Ser^{477}, and Met^{500} to estimate the roles of these amino acids.

In our previous work (*17*) we reported on another interesting observation. Mutation of Arg^{423}, which is rather distant from the ATP-binding site, had a dramatic effect on the nucleotide affinity to the N-domain. We proposed that Arg^{423} forms a hydrogen bond to Glu^{472}, and that this hydrogen bond stabilizes the shape of the whole ATP-binding pocket (*17*). Another distant residue, which could be important for the proper shape of the ATP-binding pocket, is Pro^{489}, which is conserved among P-type ATPases. To verify whether it is so, we also performed mutations of Glu^{472} and Pro^{489}.

The effect of point mutations was evaluated by the binding of the fluorescent ATP analogue TNP-ATP to the isolated N-domain. Previously, we had estimated that some mutations could affect only TNP-ATP binding but not ATP binding. Therefore, the competitive displacement of TNP-ATP by ATP was also used to test the influence of the point mutation binding of ATP.

MATERIALS AND METHODS

Construction of the Protein Expression Vector pGEX-H_4−H_5. The H_4−H_5 loop sequence was prepared by polymerase chain reaction from the sequence of the α-subunit of Na^+/K^+-ATPase from mouse brain. The construction of the expression plasmid pGEX-2T containing the cDNA for the H_4−H_5 loop (Leu^{354}−Ile^{604}) was described previously (*20*). Site-directed mutagenesis was performed by polymerase chain reaction with the QuickChange Kit (Stratagene). The upstream primers for performed mutations were (altered nucleotides are italic) (D443A) 5′-CTT AAG CGT GCA GTA GCG GGA G*C*T GCT TCC GAG TCG GCG-3′, (E472A) 5′-G TAC ACC AAG ATA GTG *T*AG ATT CCT TTC AAC TCC ACC-3′, (S477A) 5′-GTG GAG ATT CCT TTC AAC *G*CC ACC AAC AAG TAC CAG CTC TCC-3′, (P489A) 5′-CAG CTC TCC ATT CAC AAG AAC *G*CA AAC GCA TCG GAG CC-3′, (M500A) 5′-CCT AAG CAC CTG CTA GTG *GC*G AAG GGC GCC CCA GAA AGG-3′, and (R423LE472A) 5′-GA ATT GCT GGT CTC TGT AAC *CT*G GCA GTG TTT CAG GCT AAC C-3′ and primer for mutation E472A (used subsequently). The downstream primers were reverse complementary.

Expression and Purification of the H_4−H_5 Loop. The *E. coli* BL21 cells were grown to OD = 0.8 in 200 mL of LB medium containing ampicillin (50 μg/mL) at 37 °C. After addition of IPTG (final concentration 0.1 mM) the incubation continued for another 12 h at 30 °C. Centrifuged cells, resuspended in 10 mL of TENG buffer with protease inhibitors, were disrupted by sonication. Another centrifugation was performed, and the supernatant was loaded into the glutathione−Sepharose 4B column and incubated for 1.5 h at 4 °C. The fusion protein was eluted by 10 mM reduced glutathione, dialyzed for 3 h at 4 °C against the 1000-fold excess of 50 mM Tris−HCl, pH 7.5, and stored at −20 °C. Protein purity and concentration were determined by SDS−PAGE and the Bradford method (*21*), respectively.

TNP-ATP Binding to the Fusion Proteins. The fluorescence probe TNP-ATP (2′,3′-*O*-(2,4,6-trinitrophenyl)adenosine 5′-triphosphate, trisodium salt) was purchased from Molecular Probes. The emission of this fluorophore is sensitive to the polarity of its environment (*22*, *23*). Therefore, the binding of the probe to the protein could be detected as the increase of the fluorescence intensity. Aliquots of TNP-ATP were subsequently added to 1 mL of 50 mM Tris−HCl or 1 mL of 50 mM Tris−HCl containing a 1.6 μM protein solution, the mixture was gently stirred, and the fluorescence intensity was recorded after 1 min. The fluorescence intensity measurements were performed at room temperature (22 °C) using the FluoroMax-2 (Jobin Yvon/Spex) steady-state fluorometer, in 0.4 × 1 cm quartz cuvettes. Excitation and emission wavelengths were set to 462 and 527 nm, respectively, both the excitation and emission bandpasses were 10 nm, and the integration time was 5 s.

Calculation of the Dissociation Constant for TNP-ATP Binding to the Fusion Proteins. The signal of buffer and protein (if present) was collected before the addition of TNP-ATP, and this value was subtracted from all further raw data as a background. Dilution corrections of the protein and probe concentrations were calculated. The fluorescence intensity was normalized so that the fluorescence intensity of a 1 μM free probe was set to unity. The dependence of

normalized fluorescence intensity on the TNP-ATP concentration was fitted to the equation (*24*)

$$F = [P] + \frac{\gamma - 1}{2}([P] + [E] + K_P - (([P] + [E] + K_P)^2 - 4[P][E])^{1/2})$$

where F is the normalized fluorescence intensity, [P] is the concentration of TNP-ATP, [E] is the concentration of the protein, γ is the fluorescence intensity enhancement factor of the bound probe relative to the free probe, and K_P is the dissociation constant. The fluorescence intensity enhancement factor γ was estimated to be $\gamma = 2.3 \pm 0.2$. All the parameters except K_P were kept constant during the fitting procedure. All values are presented as a mean ± SEM from at least three independent measurements.

ATP Binding to the Fusion Proteins. ATP was purchased from Sigma-Aldrich (Germany). The experimental procedure was the same as for TNP-ATP binding, except that titration was performed in 1 mL of 50 mM Tris−HCl containing 20 mM ATP, pH 7.5. ATP is a weak acid and in high concentration can cause a substantial shift of pH; therefore, pH was adjusted by titration with HCl only after addition of ATP. ATP competitively displaced the TNP-ATP from the binding sites, resulting in the lower fluorescence intensity as compared to that of the titration in the absence of ATP.

Calculation of the Dissociation Constant for ATP Binding to the Fusion Proteins. The signal of buffer and protein (if present) was collected before the addition of TNP-ATP, and this value was subtracted from all further raw data as a background. Dilution corrections of the protein and probe concentrations were calculated. The fluorescence intensity was normalized as described above. The dependence of normalized fluorescence intensity on the concentration of TNP-ATP was fitted to the equation (*40*)

$$F = [P] + \frac{1}{2}(\gamma - 1)\left([P] + [E] + K_P + [A]\frac{K_P}{K_A}\left(\left([P] + [E] + K_P + [A]\frac{K_P}{K_A}\right)^2 - 4[P][E]\right)^{1/2}\right)$$

which describes the situation where probe and ATP compete for the same binding site. [A] is the total concentration of ATP, and K_A is the dissociation constant for ATP. All the parameters except K_A were kept constant during the fitting procedure. The K_P value was calculated as described above. All the K_A values are presented as the mean ± SEM of at least three independent measurements.

Thermal Stability. Purified proteins were diluted to 1 μM concentration, and the steady-state tryptophan fluorescence was monitored in the temperature range up to 65 °C. The excitation wavelength was 295 nm, both the excitation and emission band-passes were set to 3 nm, and the emission spectrum was collected with a step of 0.5 nm between 310 and 400 nm. The position of the maximum in the emission spectrum is sensitive to the polarity of the tryptophan environment and can, thus, reflect the changes the protein conformation. The plot of the emission spectrum maximum vs temperature was evaluated using a sigmoidal fit.

Preparation of the TNP-ATP Ligand for Computer Modeling. The crystal structure of TNP-ATP was extracted from the PDB coordinate file 1I5D (*25*) that is deposited in the Protein Data Bank (http://www.pdb.org). Hydrogens were added using the BIOPOLYMER module included in Insight II (Accelrys Inc., San Diego, CA).

Quantum Chemical Calculations of TNP-ATP Point Charges. Point charges applied in autodocking were solved to reproduce the electrostatic potential field determined by quantum chemical calculations. The TNP-ATP crystal structure in PDB file format was converted by the program Babel 1.6 (http://smog.com/chem/babel/) to obtain a native input file format of the electronic structure program Gaussian98 (*26*). The value of the total molecule charge was set to −3. Ab initio quantum chemical restricted Hartree−Fock single-point calculation and the 6-31G* basis set with polarization functions on heavy atoms were used to create electrostatic potential at points selected according to the Merz−Singh−Kollman scheme (*27*, *28*). The calculations provided charge fields which were consequently applied as the input for an Antechamber/RESP (*29*, *30*) (restrained electrostatic potential) software package to obtain fitting point charges consistent with the electrostatic potential.

Homology Modeling of the N-Domain and Ligand Docking. A complete model of the N-domain of mouse brain Na^+/K^+-ATPase (Arg^{378}−Asp^{586}) was generated by analogy to the crystal structure of the N-domain of porcine Na^+/K^+-ATPase (*31*, *32*). This recently published structure lacks three 6, 10, and 6 amino acid residue long loops existing in the mouse brain α_1 subunit. Hence, the three-dimensional structure of these three peptides was additionally modeled according to the procedure published previously for the H_4−H_5 loop of pig kidney Na^+/K^+-ATPase (*9*) that was in turn generated in analogy to the Ca^{2+}-ATPase (PDB code 1EUL) (*4*). The primary structure of the mouse brain Na^+/K^+-ATPase from Arg^{378} to Asp^{586} was aligned with the template sequences by CLUSTALX (*33*). The sequence alignment used for the modeling is shown in Figure 1. The three-dimensional model constituted by all non-hydrogen atoms was built and examined by the MODELLER6 package (*34*). The tertiary structure model was checked with PROCHECK (*35*). Docking of ATP and TNP-ATP as substrates was explored with the AutoDock program (*36*). Initially the substrate was placed in an arbitrary position close to the published binding site residues. With the complete preparation of the ATP ligand and the docking procedure of both substrates, we used exactly the parameters and methods published earlier (*9*).

RESULTS

Binding of TNP-ATP to the Fusion Proteins. All the mutants were expressed as GST fusion proteins in *E. coli* and purified. The purity of the proteins was checked by 12% (w/v) SDS−PAGE, and we observed a single band at 53 kDa. The expression level was high for all mutants, except for P489A mutant, which was expressed significantly less (roughly 20%; see Figure 2). However, even in this case the synthesis was sufficiently high to perform all our experiments. To verify that the GST protein itself does not bind TNP-ATP, the GST protein was incubated with TNP-ATP and the fluorescence was recorded. The fluorescence intensity of TNP-ATP in buffer was not different in the presence or absence of GST protein (not shown). Thus, there was no significant binding of TNP-ATP to GST observed over the whole range of TNP-ATP concentrations used in our study (Figure 3). Accordingly, the GST−H_4−H_5 loop fusion

```
Mouse-brain     RMTVAHMWFDNQIHEADTTENQSGVSFDKTSATWFALSRIAGLCNRAVFQANQENLPILK 437
Crystal         MMTVAHMWFDNQIHEADTT------TFDKRSPTWTALSRIAGLCNRAVF----------K
peptid1         -------------------ENQSGV-----------------------------------
peptid2         -------------------------------------------------QANQENLPIL-
peptid3         ------------------------------------------------------------
                 ******************       *** * ** **************          *

Mouse-brain     RAVAGDASESALLKCIEVCCGSVMEMREKYTKIVEIPFNSTNKYQLSIHKNPNASEPKHL 497
Crystal         RDTAGDASESALLKCIELSCGSVRKMRDRNPKVAEIS------YQLSIHEREDNPQS-HV
peptid1         ------------------------------------------------------------
peptid2         ------------------------------------------------------------
peptid3         ----------------------------------FNSTNK------------------
                *   *************  ****  **    *  **       ******         *

Mouse-brain     LVMKGAPERILDRCSSILLHGKEQPLDEELKDAFQNAYLELGGLGERVLGFCHLLLPDEQ 557
Crystal         LVMKGAPERILDRCSSILVQGKEIPLDKEMQDAFQNAYLELGGLGERVLGFCQLNLPSGK
                ******************  *** *** *  ********************* * **

Mouse-brain     FPEGFQFDTDEVNFPVDNLCFVGLISMID 586
Crystal         FPRGFKFDTDELNFPTEKLCFVGLMSMID
                ** ** ***** ***   ****** ****
```

FIGURE 1: Sequence alignment of the N-domain of the α1-subunit of mouse brain Na^+/K^+-ATPase with that of the porcine α2-subunit of Na^+/K^+-ATPase, whose tertiary structure has been solved recently at 2.6 Å resolution by X-ray crystallography and for which the PDB coordinates are available. Three 6, 10, and 6 residue long peptides from our published structure of the complete pig-kidney Na^+/K^+-ATPase were aligned to fill the gaps in the recently published structure. Identical amino acids are marked by an asterisk.

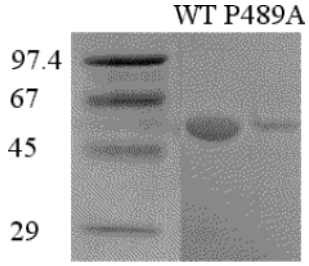

FIGURE 2: SDS−PAGE: Expression and purification of GST fusion proteins. The expression level for the P489A mutant was lower than that for the wild type. All other mutants were expressed comparably to the wild type.

protein was considered to be a suitable tool for studying the binding of TNP-ATP to the ATP-binding site. In contrast, incubation of all fusion proteins with TNP-ATP resulted in a clear and significant increase in fluorescence intensity compared to that of GST in buffer or buffer alone.

We confirmed our previous result (*16*) and estimated that the binding of TNP-ATP to the GST−[Leu^{354}−Ile^{604}] fusion protein (wild type, WT) yielded the value of the dissociation constant $K_P = 3.1 \pm 0.2$ μM (see Table 1) (*16*). We found that mutation M500A showed no alteration in TNP-ATP binding and also the mutation D443A influenced TNP-ATP binding only very slightly. On the other hand, mutation S477A led to the significant decrease of the TNP-ATP fluorescence intensity, as compared to that of the wild type, suggesting that TNP-ATP binding was prevented in this case (Figure 3). An even larger effect was observed for the E472A mutant, and interestingly, further mutation of Arg^{423} (i.e., construct R423LE472A) had no significant additional effect (Table 1). The most dramatic change was observed with the construct P489A; the TNP-ATP titration in the presence of this mutant was undistinguishable from that in the absence of any protein ($K_P > 100$ μM). The estimated dissociation constant values are sumarized in Table 1.

Binding of ATP to the GST Fusion Proteins. The dissociation constant of ATP binding to the H_4−H_5 loop of Na^+/K^+-ATPase is about 3 orders of magnitude higher than that of TNP-ATP (see Table 1). This suggests a certain stabilizing role of the trinitrophenyl moiety of the fluorescence probe in the complex with the protein. Hence, one may not exclude the possibility that the interaction of the trinitrophenyl moiety itself with the ATP-binding site is altered in our mutants. Therefore, we determined the dissociation constant of ATP−peptide complexes for all constructs as well.

Competition for the binding sites between ATP and TNP-ATP was used to characterize the binding of ATP to the fusion proteins. Notably, the presence of ATP in buffer (without any protein) did not influence the fluorescence intensity of TNP-ATP.

However, ATP changed significantly the fluorescence intensity of TNP-ATP when titrated with S477A and M500A mutants (Figure 3). The decrease in fluorescence intensity in the presence of ATP indicated that some binding sites were occupied by ATP. Notably, this effect was much smaller with the D443A, E472A, and R423L472A mutants, suggesting that the ATP was bound to these mutants very weakly. Indeed, we observed an increase of the value of the dissociation constant 6.2 ± 0.7 mM estimated for the wild type (Table 1) to 32 ± 8 mM for D443A, 20 ± 11 mM for E472A, and 35 ± 15 mM for R423LE472A. On the contrary, no significant change was observed for the mutations S477A (7 ± 1 mM) and M500A (5 ± 2 mM). The fact that mutant P489A did not significantly interact with TNP-ATP disabled the estimation of the dissociation constant for ATP binding in this case. The results of TNP-ATP and ATP binding to all mutants are summarized in Table 1.

Thermal Stability. The emission spectrum of the tryptophan fluorescence is sensitive to the polarity of the tryptophan microenvironment, which allows monitoring of the conformational changes. We observed a systematic red shift of the maximum when the temperature was increased. Notably, this effect was more pronounced for the construct containing the R423LE472A mutation than for the wild type (Figure 4). The center of the sigmoidal curve was at 54.8 °C for the wild type, but only 46.6 °C for the R423LE472A protein, suggesting that the performed mutations influenced the overall stability of the protein.

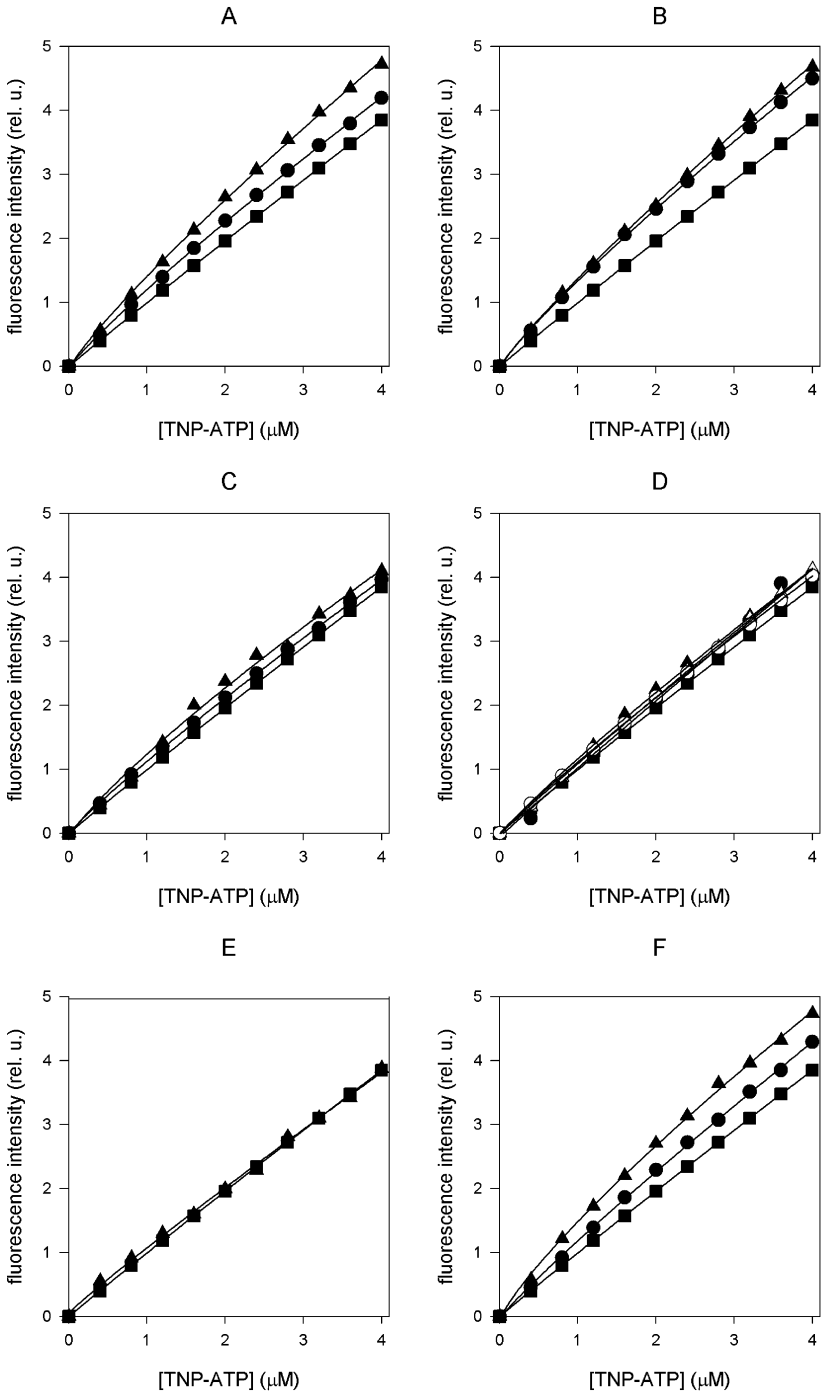

FIGURE 3: TNP-ATP binding to the H_4-H_5 loop protein with point mutations in the presence and absence of ATP, respectively. GST fusion proteins (1.6 μM) containing point mutations (A, M500A; B, D443A; C, S477A; D, E472A; E, P489A; F, wild type) were titrated with increasing amounts of TNP-ATP in 50 mM Tris−HCl, pH 7.5 (triangles). Binding of TNP-ATP resulted in an increase of the fluorescence intensity. Similar experiments were then performed in 50 mM Tris−HCl, 20 mM ATP, pH 7.5 (circles); the pH of the buffer was adjusted to 7.5 after addition of ATP. Some of the binding sites were occupied by ATP, resulting in a lower initial slope of the fluorescence intensity. For comparison, titration in pure buffer in the absence of any protein is shown (squares). Note that the same result was obtained, when only GST protein itself or ATP was present (data not shown). Open symbols in graph D represent data for the double mutant R423LE472A.

Computer Modeling. We created a structural model of the N-domain from Arg^{378} to Asp^{586} using a restraint-based comparative modeling approach. The final model had 84.9% of the residues in the most favored regions of the Ramachandran plot and an acceptable overall geometry, both determined with the ProCheck program (*35*). No residues were found in the disallowed regions. The overall *g* factor of the structure obtained showed a value of −0.31. The *g* factor should be above −0.5, and values below −1.0 may need investigation.

For the docking the Lamarckian Genetic Algorithm (GA-LS), a hybrid search technique that implements an adaptive global optimizer with a local search (*37*), was used. The global search method is a modified genetic algorithm, with

Table 1: Dissociation Constants for TNP-ATP and ATP Binding to the GST− [Leu^{354}−Ile^{604}] Fusion Proteins Are Summarized[a]

protein	K_D(TNP-ATP) (μM)	$\Delta\Delta G$(TNP-ATP) (kJ·mol^{-1})	K_D(ATP) (mM)	$\Delta\Delta G$(ATP) (kJ·mol^{-1})
wild type	3.1 ± 0.2		6.2 ± 0.7	
D443A	3.7 ± 0.2	0.4	32 ± 8	4.0
R423L[b]	18 ± 2	4.3	31 ± 9	4.0
E472A	15 ± 4	3.9	20 ± 11	2.9
R423LE472A	17 ± 5	4.2	35 ± 15	4.2
S477A	9 ± 1	2.6	7 ± 1	0.1
P489A	>100		NA[c]	
M500A	3.6 ± 0.6	0.4	5 ± 2	−0.5

[a] The presented values are the average ± SEM from at least three independent measurements. The difference in binding energies compared to that of the WT ($\Delta\Delta G$) was calculated as described in ref *41*. [b] From ref *17*. [c] Not analyzed.

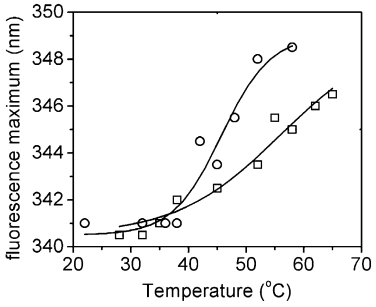

FIGURE 4: Effect of the R423LE472A mutations on the thermal stability of the N-domain. Steady-state emission spectra of the tryptophan fluorescence of the wild type (squares) and R423LE472A mutant (circles) were recorded. The position of the maximum reflected the conformational changes as a result of the temperature increase.

two-point crossover and random mutation. The local search method is based on the optimization algorithm of Solis and Wets, which modifies the phenotype.

The exploration of docking positions included for every arbitrary position 50 hybrid GA-LS docking runs using a population size of 50, a maximum number of energy evaluations of 25000, a maximum number of generations of 27000, and 300 iterations of the Solis and Wets local search. The resulting positions were clustered according to an rms criterion of 1 Å, and the most energetically favorable position of every cluster was analyzed visually to exclude artifacts. As final docking positions were selected only those positions that occur most, which means more than 20times for the 50 GA-LS docking runs. The final docked energies were −12.06 kcal/mol for ATP and −10.11 kcal/mol for TNP-ATP. This estimation of real interaction energy neglects solvation and desolvation effects and therefore cannot be compared to the dissociation constant values. However, in general, values lower than −8 kcal/mol demonstrate a binding interaction between the ligand and the substrate.

DISCUSSION

The solely expressed H_4−H_5 loop−GST fusion protein misses the interactions with other domains of the sodium pump and is not affected in its structure by Na^+- or K^+-dependent conformational changes of the transmembrane part. Moreover, it is well-known that this loop has a self-supporting structure and retains the ability to bind ATP (*18*, *38*) and to hydrolyze very slowly *p*-nitrophenyl phosphate in a Mg^{2+}-dependent way (*39*).

Recently, detailed information about the structure of the N-domain has become available. The NMR spectroscopy

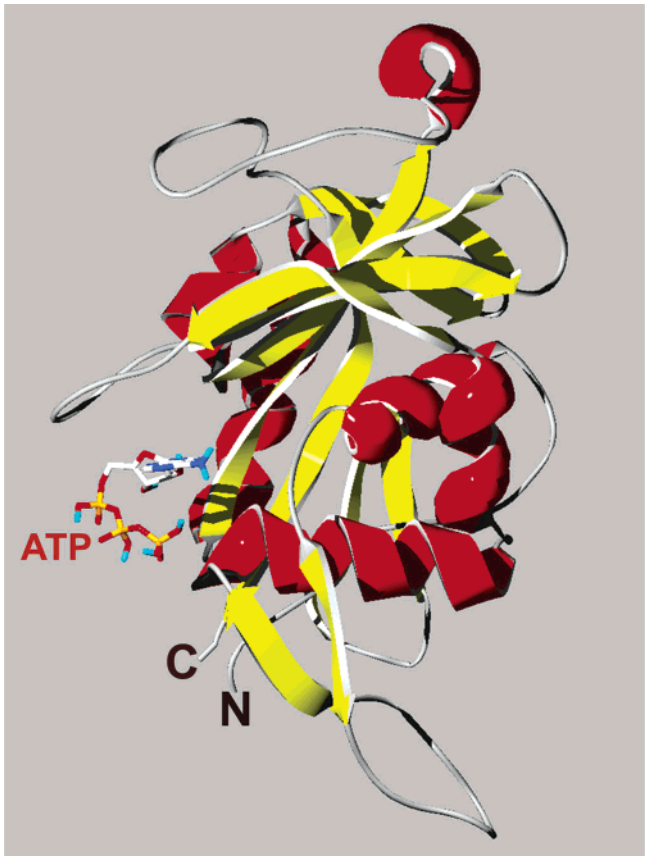

FIGURE 5: Three-dimensional representation of the complete N-domain. It has the topology of a twisted, six-stranded, antiparallel β-sheet that is flanked by two α-helices on either side. It is able to bind ATP or its analogue TNP-ATP in a well-defined binding pocket. N-terminal and C-terminal connections to the P-domain are marked N and C, respectively.

solved structure with ATP bound showed that the N-domain has the topology of a twisted, six-stranded, antiparallel β-sheet that is flanked by two α-helices on either side (Figure 5). Later also the crystal structure of the N-domain appeared, which allowed further rectification of the side chain atom position (*31*, *32*). On the other hand, the authors were unable to efficiently soak the nucleotide into the crystals. Although this structure has a good-quality stereochemistry and well-resolved side chains, three 6, 10, and 6 residue long gaps in the structure, and particularly the lack of Phe^{475} to Lys^{480} residues (which forms a substantial part of the ATP-binding pocket), made it necessary to remodel the H_4−H_5 loop structure. Only the complete region of the ATP-binding site makes the structure suitable for docking experiments, and therefore, we decided to do this modeling to be able to observe docking on an atomic level. Our new model of the mouse brain domain N from Arg^{378} to Asp^{586} shows a root-mean-square deviation (C_α) of 0.41 Å only with respect to the crystal structure.

A part of the H_4−H_5 loop of Na^+/K^+-ATPase (sequence Leu^{354}−Ile^{604}) was used to test the influence of point mutations on the binding of ATP. The fluorescent analogue of ATP, TNP-ATP, has been used to evaluate the changes of the ATP and TNP-ATP dissociation constants. Notably, all residues were replaced by residues of similar or lower polarity. This can, in principle, increase the TNP-ATP microenvironment polarity within the binding pocket and, consequently, influence the assessment of the dissociation

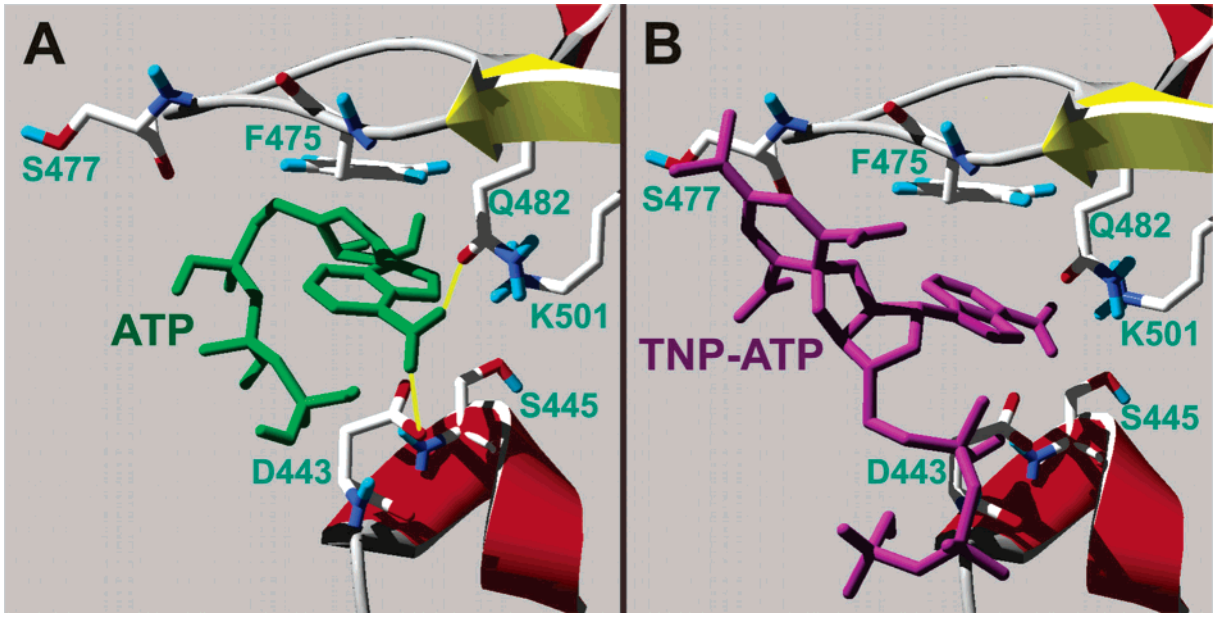

FIGURE 6: Difference in binding between ATP and TNP-ATP. (A) The most important interactions in ATP binding are the aromatic stacking between the adenosine moiety and F475 and the hydrogen bonding of its NH_2 hydrogen donor with Q482 and D443. (B) The adenosine moiety of TNP-ATP is in the opposite position compared with ATP, and its NH_2 hydrogen donor lies too much in the back of the picture to form a hydrogen bond with D443.

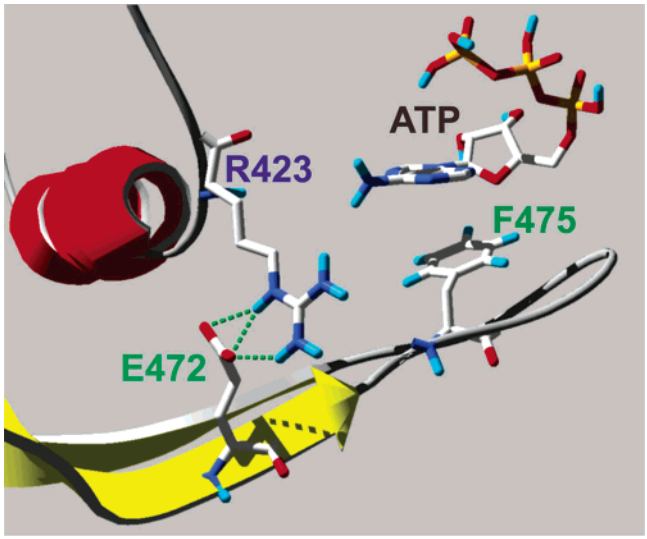

FIGURE 7: Hydrogen bond between Glu^{472} and Arg^{423}. The shape of the ATP-binding pocket is supported by a hydrogen bond between Glu^{472} and Arg^{423} that brings the stretch of amino acids containing residues Phe^{475} and Glu^{482} (not shown) close to other residues involved in ATP binding, such as Glu^{446} and Lys^{501} (not shown).

constant. Fortunately, this effect is likely to be much less than the observed difference between K_D values for the WT and most mutants. First, the ATP-binding site is composed of eight amino acids, and thus, one point mutation can hardly cause a dramatic change in its polarity. Second, we performed model calculations to show that even a relatively large error in the γ value estimation would vary the dissociation constant for ATP only moderately; e.g., increasing the γ value from 2.3 to 4.5 would increase the calculated K_D(ATP) for E472A from 20 to 24 mM only. Therefore, we could treat the fluorescence enhancement factor as a constant for all mutants.

The new model structure was taken for computational docking experiments with free ATP and TNP-ATP. In silico docking experiments identified well the ATP-binding site and resulted in binding of both substrates. The quality of our model, however, in interpreting studies of TNP-ATP and ATP binding to the H_4-H_5 loop (Table 1) had to be tested. Additionally, this model had to interpret by in silico docking experiments (Figure 6) the observed changes in terms of interaction with specific amino acids (Table 1).

As we have shown recently, besides the previously reported amino acids Lys^{480}, Lys^{501}, and Gly^{502}, also Glu^{446}, Phe^{475}, and Gln^{482} form the ATP-recognizing pocket of Na^+/K^+-ATPase (*16*, *17*, *24*). The NMR structure of the N-domain confirmed the close proximity of all these residues to the ATP-binding site and detected a hydrogen bond between Gln^{482} and the adenosine moiety (*18*). In our previous work we reported that mutation of Arg^{423} resulted in a strong inhibition of both TNP-ATP and ATP binding (K_D(TNP-ATP) = 18 ± 2 μM and K_D(ATP) = 31 ± 10 mM) (*17*). This was rather surprising because this residue is 7 Å from the bound ATP molecule and lies outside the binding pocket (*9*). Hence, we proposed that this residue might stabilize the shape of the ATP-binding pocket by a hydrogen bond to Glu^{472} over a distance of 1.7 Å.

To verify this hypothesis, we also mutated Glu^{472} to see whether this mutation would have an effect similar to that of the mutation of Arg^{423}. Indeed, a strong decrease of nucleoside triphosphate binding was observed for TNP-ATP (K_D = 15 ± 4 μM) and ATP (K_D = 20 ± 10 mM) binding, and the values matched within the range of error values estimated for Arg^{423}. Moreover, the performance of the R423L mutation on the construct already containing the E472A mutation (i.e., the R423LE472A construct) did not bring any significant effect on both TNP-ATP (17 ± 5 μM) and ATP (35 ± 15 mM) binding, and the values match well the values obtained for the R423L mutant. Thus, we can see that these two mutations has no additive effect on the nucleotide binding, and this finding strongly supports the suggestion that a hydrogen bond exists between Arg^{423} and Glu^{472} (Figure 7). Such information is beyond the resolution

of both the N-domain structures mentioned above. Breaking this hydrogen bond leads to instability in the stretch of amino acids containing the residue Phe[475], Lys[480], or Gln[482] within the binding pocket, which are in proximity of the other residues involved in ATP binding, such as Lys[501] or Glu[446]. This corresponds to our observation that mutations of Arg[423] and Glu[472] affected the thermal stability of the N-domain and also to the finding that mutations of Glu[472] lead to a strong inhibition of Na^+/K^+-ATPase (*14*).

Even more dramatic changes were observed after mutation of the conserved residue Pro[489]. We were not able to detect any TNP-ATP binding, suggesting that the performed mutation substantially influenced the structure of the nucleotide-binding site. Indeed, Pro[489] is located on the loop connecting the third and fourth β-strands of the N-domain. Proline is the only residue that forces the peptidic backbone to adopt the cis conformation. Thus, its replacement by any other amino acid probably results in the change of the mutual position of the third and fourth β-sheets. The third β-strand contains residues Lys[480] and Gln[482], while the fourth β-strand contains the segment Lys[501]−Ala[503]. Proper mutual position of these residues is required for the effective ATP recognition. Thus, the Pro[489] mutation affects the backbone forming the ATP site rather indirectly, similarly to what was discussed for Arg[423] and Glu[472] in the previous paragraph.

Mutation of Ser[477] resulted in a moderate change of the dissociation constant for TNP-ATP binding, whereas ATP binding was not affected at all (Table 1). Although this residue is localized more than 4.1 Å away from ATP, its closest distance from the Meissenheimer complex of TNP-ATP is only 2.5 Å. We therefore must conclude that Ser[477] interacts with the trinitrophenyl residue of the more bulky TNP-ATP.

However, such an argument failed in the case of the Asp[443] mutation (Table 1). Surprisingly, we observed practically no difference in TNP-ATP binding, while the binding of pure ATP was strongly suppressed. In silico docking of both substrates revealed that the position of the ATP in the binding pocket is not precisely the same as the position of the adenosine triphosphate part of TNP-ATP (Figure 6). The aromatic stacking interaction between the adenosine moiety and Phe[475] and hydrogen bonding of the adenosine NH_2 hydrogen donor were described to be the most important interactions between ATP and the protein (*16*−*18*). On the basis of molecular modeling of both substrates in the binding pocket, we hypothesize the existence of the direct hydrogen bonding of the 6-NH_2 group of the adenine moiety with Gln[482] and Asp[443] in the case of ATP. It must be added that three-dimensional fitting of the NMR structure and our modeled structure, both with bound ATP, shows that the adenosine NH_2 hydrogen donor in both structures is in nearly the same position, only 0.8 Å from each other. TNP-ATP, however, lies indeed in a slightly different orientation in the binding pocket, and we are unable to observe hydrogen bonding of its 6-NH_2 hydrogen donor. Note that Asp[443] is approximately 6 Å from the adenosine moiety in the NMR structure, which makes the direct interaction rather unlikely. However, if one compares the binding pocket of the crystal structure with that of both NMR structures, a discrepancy in the position of D443 (D450 in the NMR structures) is found. The carboxyl group of the D443 in the crystal structure is 2.7 Å from the position in the NMR structure without ATP and 3.4 Å with ATP. Moreover, already recently published mutagenesis (*42*) and iron-oxidative cleavage (*43*) experiments suggested the importance of this residue for ATP binding. This discrepancy could reflect different transient subconformations of the protein and/or some segmental dynamics. However, explanation of the discrepancy between the NMR structure and other experiments may need further investigation.

Mutation of Met[500] altered neither TNP-ATP nor ATP binding. Thus, although the peptide backbone of this residue is 6.1 Å from the ATP molecule, its side chain is probably buried under the surface and its mutation cannot influence ligand binding.

In conclusion, we have proven that a hydrogen bond between Arg[423] and Glu[472] supports the connection of two opposite halves of the ATP-binding pocket. Similarly, the conserved residue Pro[489] is substantial for the proper interaction of the third and fourth β-strands, which both contain residues that take part in ATP binding. Mutation of Asp[443] suggested that TNP-ATP and ATP adopt different positions in the nucleotide-binding pocket. On the basis of the recently published crystal structure, we improved our model and computed the interaction of these two ligands with the N-domain. This model is in agreement with all previously reported spectroscopic data and revealed that Asp[443] forms a hydrogen bond with the 6-NH_2 group of the adenosine moiety of ATP, but not TNP-ATP.

ACKNOWLEDGMENT

We thank K. O. Håkansson for providing the atomic coordinates of the Na^+/K^+-ATPase N-domain crystal structure.

REFERENCES

1. Kaplan, J. H. (2002) Biochemistry of Na,K-ATPase, *Annu. Rev. Biochem. 71*, 511−535.
2. Jorgensen, P. L., Hakansson, K. O., and Karlish, S. J. D. (2003) Structure and mechanism of Na,K-ATPase: Functional Sites and Their Interactions, *Annu. Rev. Physiol. 65*, 817−849.
3. Geering, K. (1996) Oligomerization and maturation of eukaryotic membrane proteins, in *Membrane Assembly, Molecular Biology Intelligence Unit Sereis* (Van Heijne, G., Ed.) pp 173−188, Landes Co., New York.
4. Toyoshima, C., Nakasako, M., Nomura, H., and Ogawa, H. (2000) Crystal structure of the calcium pump of sarcoplasmic reticulum at 2.6 Angström resolution, *Nature 405*, 647−655.
5. Toyoshima, C., and Nomura, H. (2002) Structural changes in the calcium pump accompanying the dissociation of calcium, *Nature. 418*, 605−611.
6. Rice, W. J., Young, H. S., MArtin, D. W., Sachs, J. R., and Stokes, D. L. (2001) Structure of Na^+/K^+-ATPase at 11 A resolution: Comparison with Ca^{2+}-ATPase in E1 and E2 states, *Biophys. J. 80*, 2187−2197.
7. Sweadner, K. J., and Donnet, C. (2001) Structural similarities of Na,K-ATPase and SERCA, the Ca^{2+}-ATPase of the sarcoplasmic reticulum, *Biochem. J. 356*, 685−704.
8. Patchornik, G., Munson, K., Goldshleger, R., Shainskaya, A., Sachs, G., and Karlish, S. J. D. (2002) The ATP-Mg^{2+} binding site and cytoplasmic domain interactions of Na^+,K^+-ATPase investigated with Fe^{2+}-catalyzed oxidative cleavage and molecular modeling, *Biochemistry 41*, 11740−11749.
9. Ettrich, R., Melichercik, M., Teisinger, J., Ettrichova, O., Krumscheid, R., Hofbauerova, K., Kvasnicka, P., Schoner, W., and Amler, E. (2001) Three-dimensional structure of the large cytoplasmic H_4-H_5-loop of Na^+/K^+-ATPase deduced by restraint-based comparative modeling shows only one ATP-binding site, *J. Mol. Model. 7*, 184−192.

10. Tran, C. M., Huston, E. E., and Farley, R. A. (1994) Photochemical labeling and inhibition of Na,K-ATPase by 2-Azido-ATP. Identification of an amino acid located within the ATP binding site, *J. Biol. Chem. 269*, 6558−6565.
11. Tran, C. M., Scheiner-Bobis, G., Schoner, W., and Farley, R. A. (1994) Identification of an amino acid in the ATP binding site of Na^+/K^+-ATPase after photochemical labeling with 8-azido-ATP, *Biochemistry 33*, 4140−7.
12. Farley, R. A., Tran, C. M., Carilli, C. T., Hawke, D., and Shively, J. E. (1984) The amino acid sequence of a fluorescein-labeled peptide from the active site of (Na,K)-ATPase, *J. Biol. Chem. 259*, 9532−9535.
13. Amler, E., Abbott, A., and Ball, W. J. J. (1992) Structural dynamics and oligomeric interactions of Na,K-ATPase monitored using fluorescence energy transfer, *Biophys. J. 61*, 553−568.
14. Scheiner-Bobis, G., and Schreiber, S. (1999) Glutamic acid 472 and Lysine 480 of the sodium pump α1 subunit are essential for activity. Their conservation in pyrophosphatases suggests their involvement in recognition of ATP phosphatases, *Biochemistry 38*, 9198−9208.
15. Teramachi, S., Imagawa, T., Kaya, S., and Taniguchi, K. (2002) Replacement of several single amino acid side chains exposed to the inside of the ATP-binding pocket induces different extents of affinity change in the high and low affinity ATP-binding sites of rat Na/K-ATPase., *J. Biol. Chem. 277*, 37394−37400.
16. Kubala, M., Hofbauerova, K., Ettrich, R., Kopecky, V., Krumscheid, R., Plásek, J., Teisinger, J., Schoner, W., and Amler, E. (2002) Phe^{475} and Glu^{446} but not Ser^{445} participate in ATP binding to the α-subunit of Na^+/K^+-ATPase, *Biochem. Biophys. Res. Commun. 297*, 154−159.
17. Kubala, M., Teisinger, J., Ettrich, R., Hofbauerová, K., Kopecký, V., Baumruk, V., J., P., Schoner, W., and Amler, E. (2003) Eight amino acids are forming the ATP recognition site of Na^+/K^+-ATPase, *Biochemistry 42*, 6446−6452.
18. Hilge, M., Siegal, G., Vuister, G. W., Güntert, P., Gloor, S. M., and Abrahams, J. P. (2003) ATP-induced conformational changes of the nucleotide-binding domain of Na, K.-ATPAse, *Nat. Struct. Biol. 10*, 468−474.
19. Abu-Abed, M., Mal, T. K., Kainosho, M., MacLennan, D. H., and Ikura, M. (2002) Characterization of the ATP-binding domain of the sarco(endo)plasmic reticulum Ca^{2+}-ATPase: probing nucleotide binding by multidimensional NMR, *Biochemistry 41*, 1156−1164.
20. Hofbauerova, K., Kopecky, V. J., Ettrich, R., Ettrichova, O., and Amler, E. (2002) Secondary and tertiary structure of nucleotide-binding domain of alpha subunit of Na^+/K^+-ATPase, *Biopolymers 67*, 242−246.
21. Bradford, M. M. (1976) A rapid and sensitive method for the quantitation of microgram quantities of protein utilizing the prinziple of protein-dye binding, *Anal. Biochem. 72*, 248−254.
22. Hiratsuka, T., Sakata, I., and Uchida, K. (1973) Synthesis and properties of N6-(2,4-dinitrophenyl)-adenosine 5′-triphosphate, an analogue of ATP, *J. Biochem. (Tokyo) 74*, 649−659.
23. Hiratsuka, T., and Uchida, K. (1973) Preparation and properties of 2′(or 3′)-O-(2,4,6-trinitrophenyl) adenosine 5′-triphosphate, *Biochim. Biophys. Acta 320*, 635−647.
24. Kubala, M., Plasek, J., and Amler, E. (2003) Limitations in linearized analyses of binding equilibria: binding of TNP-ATP to the H_4-H_5 loop of Na/K-ATPase, *Eur. Biophys. J. 32*, 363−369.
25. Bilwes, A. M., Quezada, C. M., Croal, L. R., Crane, B. R., and Simon, M. I. (2001) Nucleotide binding to histidine kinase Chea, *Nat. Struct. Biol. 8*, 353.
26. Frisch, M. J., Trucks, G. W., Schlegel, H. B., Scuseria, G. E., Robb, M. A., Cheeseman, J. R., Zakrzewski, V. G., Montgomery, J. A., Stratmann, J. R. E., Burant, J. C., Dapprich, S., Millam, J. M., Daniels, A. D., Kudin, K. N., Strain, M. C., Frakas, O., Tomasi, J., BArone, V., Cossi, M., Cammi, R., Mennucci, B., Pomelli, C., Adamo, C., Clifford, S., Ochterski, J., Peterson, G. A., Ayala, P. Y., Cui, Q., MArokuma, K., Malick, D. K., Rabuck, A. D., Raghavachari, K., Foresman, J. B., Cioslowski, J., Ortiz, J. V., Baboul, A. G., Stefanov, B. B., Liu, G., Liashenko, A., Piskorz, P., Komaromi, I., Gompertz, R., MArtin, R. L., Fox, D., Keith, T., Al-Laham, M. A., Peng, C. Y., Nanayakkara, A., Challombe, M., Gill, P. M. W., Johnson, B., Chen, W., Wong, M. W., Andres, J. L., Gonzales, C., Head-Gordon, M., Replogle, E. S., and Pople, J. A. (1998) Gaussian 98, Revision A.9, Gaussian, Inc., Pittsburgh, PA.
27. Besler, B. H., Merz, J. K. M., and Kollmann, P. A. (1990) Atomic charges derived from semiempirical methods, *J. Comput. Chem. 5*, 431.
28. Singh, U. C., and Kollman, P. A. (1984) An approach to computing electrostatic charges for molecules, *J. Comput. Chem. 5*, 129.
29. Wang, J., Wang, W., and Kollman, P. A. (2001) Antechamber, an Accessory Software Package for Molecular Mechanical Calculations, *Abstr. Pap.—Am. Chem. Soc. 222*, 135-COMP Part 1.
30. Cornell, W. D., Cieplak, P., Bayly, C. I., Gould, I. R., Merz, K. M., Ferguson, D. M., Spellmeyer, D. C., Fox, T., Caldwell, J. W., and Kollmann, P. A. (1995), *J. Am. Chem. Soc. 117*, 5179−5197.
31. Hakansson, K. O. (2003) The Crystallographic Structure of Na,K-ATPase N-domain at 2.6 Å Resolution, *J. Mol. Biol. 332*, 1175−1182.
32. Haue, L., Pedersen, P. A., Jorgensen, P. L., and Hakansson, K. O. (2003) Cloning, expression, purification and crystallization of the N-domain from α_2 subunit of the membrane-spanning Na,K-ATPAse protein, *Acta Crystallogr., D 59*, 1259−1261.
33. Thompson, J. D., Gibson, T. J., Plewniak, F., Jeanmougin, F., and Higgins, D. G. (1997) The ClUSTAL_X windows interface: flexible strategies for multiple seqeunce alignment aided by quality analysis tools, *Nucleic Acids Res. 25*, 4876.
34. Sali, A., and Blundell, T. L. (1993) Comparative protein modelling by satisfaction of spatial restraints., *J. Mol. Biol. 234*, 779−815.
35. Laskowski, R. A., McArthur, M. W., Moss, D. S., and Thornton, J. M. (1993) Prosche—a program to check the stereochemical quality of protein structures, *J. Appl. Crystallogr. 26*, 283−291.
36. Morris, G. M., Goodsell, D., Huey, R., and Olson, A. J. (1996) Distributed automated docking of flexible ligands to proteins: Parallel applications of AutoDock 2.4, *J. Comput.-Aided Mol. Des. 10*, 293−304.
37. Solis, F. J., and Wets, R. J. (1981) Minimization by random research techniques, *Math. Opr. Res. 6*, 19−30.
38. Gatto, C., Wang, A. X., and Kaplan, J. H. (1998) The M_4M_5 cytoplasmic loop of the Na,K-ATPase, overexpressed in *Escherichia coli*, binds nucleoside triphosphates with the same selectivity as the intact native protein, *J. Biol. Chem. 273*, 10578−10585.
39. Tran, C. M., and Farley, R. A. (1999) Catalytic actvivity of an isolated domain of Na,K-ATPase expressed in *Escherichia coli*, *Biophys. J. 77*, 258−266.
40. Kubala, M., Plasek, J., and Amler, E. (2004) Fluorescence competition assay for the assessment of ATP binding to an isolated domain of Na^+,K^+-ATPase, *Physiol. Res. 53* (1), 109−113.
41. Pedersen, P. A., Jorgensen, J. R., and Jorgensen, P. L. (2000) Importance of conserved alpha-subunit segment 709GDGVND for Mg^{2+} binding, phosphorylation, and energy transduction in Na,K-ATPase, *J. Biol. Chem. 275*, 37588−95.
42. Imagawa, T., Shunji K., and Taniguchi K. (2003) The amino acid sequence 442GDASE446 in Na/K-ATPase is an important motif in forming the high and low affinity ATP binding pockets, *J. Biol. Chem. 278*, 50283−50292.
43. Patchornik G., Munson K., Goldshleger R., Shainskaya A., Sachs G., Karlish S. J. (2002) The ATP-Mg^{2+} binding site and cytoplasmic domain interactions of Na^+,K^+-ATPase investigated with Fe^{2+}-catalyzed oxidative cleavage and molecular modeling, *Biochemistry 41*, 11740−9.

BI0496485